Original Article

Synthesis, antioxidant activity, and density functional theory study of some novel 4-[(benzo[*d*]thiazol-2-ylimino)methyl]phenol derivatives: a comparative approach for the explanation of their radical scavenging activities

Mohammad hossein Asgarshamsi[1], Afshin Fassihi[1,*], Farshid Hassanzadeh[1], Lotfollah Saghaei[1], Ahmad Movahedian Attar[2], and Hossein Mohammad-Beigi[3]

[1]*Department of Medicinal Chemistry, School of Pharmacy and Pharmaceutical Sciences, Isfahan University of Medical Sciences, Isfahan, I.R. Iran.*
[2]*Department of Biochemistry, School of Pharmacy and Pharmaceutical Sciences, Isfahan University of Medical Sciences, Isfahan, I.R. Iran.*
[3]*The Centre for Cellular Signal Patterns (CellPAT), Gustav Wieds vej 14, 8000 Aarhus C, Denmark.*

Abstract

Background and purpose: Radicals produced by Fenton and Haber-Weiss reactions play detrimental roles in our body. Some oxidized proteins as toxic configurations are identified in amyloid-β deposits. These deposits mostly occur in conditions, such as Alzheimer's disease. Here, we report the synthesis, evaluation of the antioxidant activity, and implementation of density functional theory (DFT) calculations of some4-[(benzo[*d*]thiazol-2-ylimino) methyl]phenol derivatives. The aim of this study was to provide a comparative theoretical-experimental approach to explain the antioxidant activities of the compounds.

Experimental approach: Compounds were synthesized by the reaction between *para* hydroxybenzaldehyde and aminobenzothiazole derivatives. The scavenging activity of the compounds was evaluated. Various electronic and energetic descriptors such as high occupied molecular orbital and low unoccupied molecular orbital energy gaps, bonding dissociation enthalpy of OH bond, ionization potential, electron affinity, hardness, softness, and spin density of the radical and neutral species were calculated. DFT calculations with B3LYP hybrid functional and 6-311++ G** basis set in the polarizable continuum model were utilized to obtain these descriptors.

Findings/Results: Ascorbic acid showed the best DPPH scavenging activity. However, **4d** and **4c** showed promising antioxidant activity. The values of E_{HOMO} for **4c** and **4d** were closer to zero, thus, they showed the best scavenging activities. The computational results were in accordance with the experimental ones. The energetic descriptors indicated that the sequential proton loss-electron transfer mechanism is preferred over other mechanisms.

Conclusion and implication: Antioxidant activity of 4-[(Benzo[*d*]thiazol-2-ylimino) methyl]phenol derivatives confirmed by experimental and theoretical documents proves them as novel antioxidants against amyloid-β based disease.

Keywords: Aminobenzothiazole; Amyloid-β; Antioxidant; Density functional theory.

INTRODUCTION

Fenton and Haber-Weiss terms are well-known in oxidative reactions. Metal ions such as Fe^{3+} and Cu^+ generate reactive oxygen radicals through the Fenton and Haber-Weiss reactions. The reduced form of transition-metal (M^{n+}) reacts through the Fenton reaction with hydrogen peroxide, leading to the generation of hydroxyl radicals. In the Haber-Weiss reaction, superoxide radical anion ($O_2{\bullet}-$), producedfrom the reduction of oxygen by a single electron,

*Corresponding author: A. Fassihi
Tel: +98-3137927100, Fax: +98-*3136680011*
Email: fassihi@pharm.mui.ac.ir

reacts with the oxidized form of transition metals ($M^{(n+1)}$) leading to the production of M^{n+}, which again affects the redox cycling (1). Hydrogen peroxide, hydroxyl radicals, and superoxide radical anion are regarded as common examples of reactive oxygen species (ROSs) for their extreme tendency to react with the molecules and biomolecules in the environment. In biologic media, they react readilywithaminoacids,lipids, carbohydrates, and DNA to achieve more stability. This causes oxidative damages and an increase in ROS levels eventually leads to destructive effects on cell functions and homeostasis (2). This happens when the concentration of ROS exceeds the capacity of the endogenous and exogenous anti-oxidative protection systems of the body, a phenomenon called oxidative stress.

Antioxidants are compounds which inhibit oxidation by transferring one electron to the ROSs to block their reactivity, thus they are also called 'scavengers'. Antioxidants can inhibit oxidative chain reactions in several ways including direct scavenging of ROSs, inhibition or stimulation of enzymes involved in oxidative reactions of the body, and chelation of metal ions such as Fe^{3+} and Cu^+.

Amyloid-beta (Aβ) deposits are of abnormal protein structures. They are often produced from the interaction of toxic protein configurations with other native copies of the same protein and catalysis of their transition state into a toxic state (3). Aβ deposition mostly occur in neurodegenerative conditions, such as Alzheimer's disease, Parkinson's disease, type I diabetes mellitus, and Huntington disease (4). In the early stages of Alzheimer's disease, some oxidized proteins as toxic configurations are also identified in brain regions rich with Aβ deposits as the tissue manifestations of the disease. In Alzheimer's disease-affected brains, high concentrations of Cu, Zn, and Fe co-localize in the Aβ deposits (5). This rapidly facilitates aggregation through binding to three histidines in the Aβ structure (H6, H13, and H14). Metal-histidine bindings generate ROS through the Fenton and Haber-Weiss reactions (6).

Designing of some multi-target scaffolds for the treatment of Alzheimer's disease was performed in the past, for example in 2012, a series of novel resveratrol derivatives were synthesized as neuroleptic, Aβ1-42 aggregation inhibitors, and antioxidant (7). Indeed, in 2016 novel indandiones were designed and synthesized. Some of them displayed promising antioxidant activity and neuroprotection in the cell (8).

For the delivery of an antioxidant substance to the regions rich with Aβ deposits, one targeting moiety should be present in the compound. Benzothiazole, for example, is a scaffold that sterically "locks" the thioflavin t-binding site in amyloid fibrils (9). On the other hand, stilbene-like scaffolds such as resveratol and curcumin, have shown a promising effect on Aβ aggregationinhibitoryactivity. antioxidant pharmacophore of resveratrol is 4-hydroxystilbene. In this structure, the π-type electron system determines the of radicals and the unpaired electrons are mostly distributed to the O-atom in the para position, double bond, and B-benzene ring (Scheme 1).
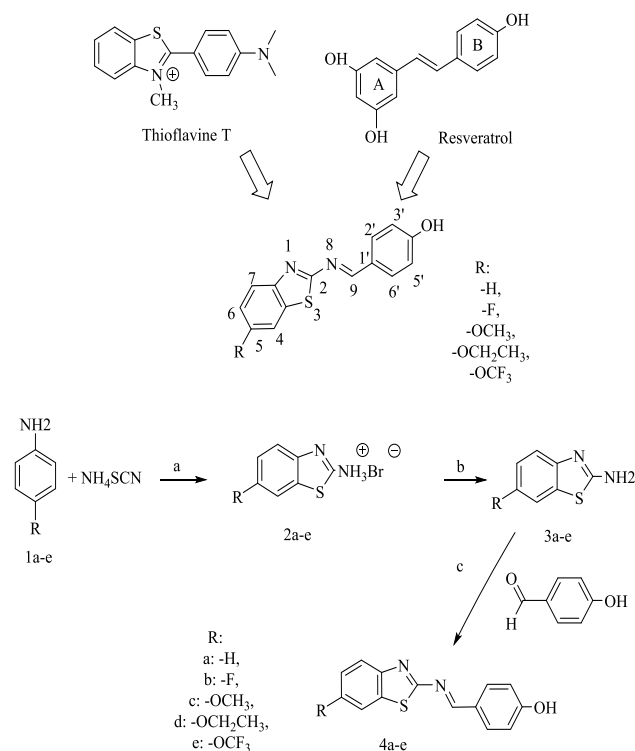
Scheme 1. Rational design, the numbering method, and synthesis for (benzo[*d*]thiazol-2-ylimino) methyl derivatives. (a) Br$_2$ in acetic acid, ice bath, 5 h; (b) NH4OH (26%); (c) *para*-hydroxy benzaldehyde, acetic acid, chloroform, 70 °C, 20 h.

The antioxidant activity of resveratrol is related to the stabilization energy of the 4-hydroxystilbene in these compounds (10,11).

In the present study, some hybrid compounds with a benzothiazole ring in their structure as a targeting moiety were designed. Half of the 4-hydroxystilbene moiety, including the aza-analogue of the styrene which is attached to the benzothiazole part, is also merged in the designed structure (Scheme 1). To reach the optimal radical scavenging ability, the C-6 position of the benzothiazole ring was substituted. Considering the bioisosterism concept, one part of the molecule represented in Scheme 1 might be considered as an equivalent of the 4-hydroxystilbene moiety. All the designed structures were synthesized and their radical scavenging ability was investigated using 2,2-diphenyl-1-picryl-hydrazyl-hydrate (DPPH) method. The experimental results were compared with the results obtained by the density functional theory (DFT) approach.

MATERIAL AND METHODS

Chemistry

Chemicals and solvents were obtained from Sigma-Aldrich (USA) and Samchun chemical companies (South Korea). Solvents were dried and purified by standard procedures. Melting points (mp) were determined in Thermo Fisher scientific IA9200 apparatus (USA). Infra-red (IR) spectra were measured on Perkin Elmer spectrophotometer (USA) with potassium bromide (KBr) as diluent. 1H-NMR and 13C-NMR spectra were recorded on a Bruker Avance 400 MHz spectrometer (USA) in deuterated-dimethyl sulfoxide (DMSO-d_6) solvent with tetramethylsilane (TMS) as the internal standard. Chemical shifts δ were reported in ppm downfield to TMS and coupling constants values (J) were estimated in Hertz (Hz). Mass spectra were recorded on Agilent 5975c-inert MSD with the Triple-Axis Detector spectrometer. Reactions were monitored using thin-layer chromatography (TLC) on pre-coated silica gel 60F254 TLC plates obtained from Merck Chemicals (Germany). The procedure for the synthesis of 4-((benzo[d]thiazol-2-ylimino)methyl)phenol derivatives (**4a-e**) is provided in Scheme 1.

Synthesis of 2-amino substituted benzothiazole scaffolds(3a-e)

The titled compounds were prepared through three steps from aniline derivatives as the starting material. Benzo[d]thiazol-2-amine derivatives (**3a-e**) were prepared according to the method reported by Jimonet *et al*. (12)

According to the Jimonet *et al*. method, aniline derivatives (0.03 mol), 95% acetic acid (45 mL), and ammonium thiocyanate (0.12 mol) were slowly added to a solution of bromine (1.5 mL; 0.03 mol) in acetic acid (20 mL) and stirred for 21 h at room temperature. When the reaction finished the mixture was poured into cold water (600 mL) and the pH was adjusted to 7 using 26% aqueous ammonia and the product was extracted with ethyl acetate (50 mL) three times. Organic layers were collected and evaporated. The obtained product was crystallized from ethanol:ether (10:90) to yield benzo[d]thiazol-2-amine derivatives. Crystals were dried under a vacuum at 40 °C for 24 h (14).

Synthesis of 4-((benzo[d]thiazol-2-ylimino) methyl)phenol derivatives (4a-e)

Each of benzo[d]thiazol-2-amine derivatives (2 mmol) was dissolved in 15 mL chloroform. Then three drops of glacial acetic acid were added. *Para*-hydroxy benzaldehyde was added to this mixture. The mixture was subsequently refluxed and the progression of the reaction was monitored by TLC. The reaction was completed within 20 h. The product was filtrated off, washed with cold diethyl ether, dissolved in acetone, and precipitated using petroleum ether, and finally recrystallized in absolute ethanol. The obtained crystals were washed again with diethyl ether and dried under vacuum. The compounds were characterized using IR, proton nuclear magnetic resonance (^{1}HNMR), carbon nuclear magnetic resonance (^{13}CNMR), and mass spectroscopic methods.

DPPH radical scavenging activity assay

This assay was performed according to the already reported method (13). Briefly, 4 mL of different concentrations of methanolic solution of standard or test compounds (10 to 2000 mM) was added to 2 mL of DPPH methanolic solution (60 mM). The mixture was shaken vigorously and allowed to stand for 30 min, and then the

absorbance of the resulting solution was measured at 517 nm using a UV/Vis spectrophotometer. Scavenging of DPPH free radicals was calculated as:

$$\%DPPH\ Scavenging = \left(\frac{Ac-At}{Ac}\right) \times 100 \qquad (1)$$

where, Ac is the absorbance of the control tube (containing all reagents except the test compound), and At is the absorbance of the test tube. Ascorbic acid was used as standard.

Computational methods

The electron densities of molecules were determined using the DFT methodology. The approach of the Lee, Yang, and Parr correlation functional in combination with Becke three-parameter exchange functional (B3LYP) was applied in the calculations (14). Molecular structures of phenolic antioxidants and their equivalent free radicals, anions, and radical cations were optimized with the 6-311++G** basis set implemented in the Gaussian 03 program (15). The calculated structures represent global minima at the potential energy surface which were established *via* frequency calculations. Self-consistent reaction field polarizable continuum model (PCM) was used to imitate the influence of water solvation on the chemical properties.

Global descriptive parameters for compounds 4a-e

Preliminary, the single occupied molecular orbital (SOMO) of radical species of the studied compounds were plotted (16). Then, using the frontier molecular orbital theory, some electronic properties including first ionization potential (IP), electron affinity (EA), energy gap (Egap), hardness (η), and softness (S) were calculated. Koopman's theorem can well approximate the electron donating capacity by the negative of the highest occupied molecular orbital (HOMO) energy (17).

$$IP = -E_{HOMO} \qquad (2)$$

The evaluation of the electron-accepting capacity by EA parameter using negative of the lowest unoccupied molecular orbital (LUMO) energy is also possible.

$$EA = -E_{LUMO} \qquad (3)$$

The ability of the compound to participate in oxidation-reduction reactions was characterized using Egap (the difference between E_{HOMO} and E_{LUMO}). Indeed, the chemical η and S are calculated using the below equations (18):

$$H = (IP - EA)/2 \qquad (4)$$

$$S = 1/(2\eta) \qquad (5)$$

Neutral bond orbital analysis

Neutral bond orbital (NBO) analysis was performed to investigate molecular orbital population analysis, and delocalization of electron density from occupied Lewis-type (donor) NBOs to unoccupied non-Lewis type (acceptor) NBOs. Perturbation analysis is also an efficient method to study the charge transfer or conjugative interactions in a molecular system (19).

Analysis of antioxidant capacity

The phenolic group in these compounds generally exhibits antioxidant activity by three different mechanisms (20). The first mechanism involves hydrogen atom transfer (HAT) from the phenolic hydroxyl group:

$$ArOH + R\bullet \rightarrow ArO\bullet + RH \qquad (I)$$

Bond dissociation enthalpy (BDE) is a numerical parameter related to HAT mechanism which is calculated using the electronic and thermal enthalpies as follows:

$$BDE = Hr + Hh - Hn \qquad (6)$$

where Hr is the enthalpy of the radicals generated through H-atom abstraction, Hh is the enthalpy of the hydrogen atom, which is -4 KJ/mol and Hn is the enthalpy of the neutral compound.

Electron and then proton transfer (SET-PT) from the phenolic hydroxyl oxygen is the other antioxidant mechanism:

$$ArOH + R\bullet \rightarrow ArOH^{\bullet+} + R^-$$
$$ArOH^{\bullet+} + R^- \rightarrow ArO^\bullet + RH \qquad (II)$$
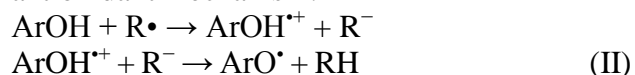
Adiopathic ionization potential (AIP) and proton dissociation enthalpy (PDE) are numerical parameters related to the SET-PT mechanism as follows:

$$AIP = Hrad.cat + He - Hn \qquad (7)$$

$$PDE = Hr + Hpro - Hrad.cat \qquad (8)$$

where Hr is the enthalpy of radical, Hrad.cat is the enthalpy of radical cation, and Hpro is the proton enthalpy, which is -1090 kJ/mol.

And finally, sequential proton loss-electron transfer (SPLET) in which:

$$ArOH \rightarrow ArO^- + H^+ \qquad (III)$$
$$ArO^- + R^\bullet \rightarrow ArO^\bullet + R^- \qquad (IV)$$
$$R^- + H^+ \rightarrow RH$$
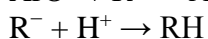
where, the electron-transfer enthalpy (ETE) and proton affinity (PA) are numerical parameters related to the SPLET mechanism as follows (21):

$$PA = Han + Hpro - Hn \qquad (9)$$

$$ETE = Hr + He - Han \qquad (10)$$

In this equation, Han is the enthalpy of the anion and He is the enthalpy of the electron, which is -105 kJ/mol.

Spin density analysis

In all the three mechanisms described above, the neutral compound (ArOH) is converted to a common free radical (ArO·), which is more stable and less reactive than other radical species (R). Thus, the spin density distribution of all derivatives was analyzed for common free radical (ArO·).

In order to rationalize the differences in reactivity of the OH sites and the BDE differences, the distribution of electron spin over the whole structure of each radical (ArO.) was investigated. Higher delocalization of the spin density in the radical is in agreement with the easier formation of the radical (22).

RESULTS

Chemistry

The corresponding data for compounds **1a-e**, **2a-e**, and **3a-e** were reported previously (12). Thus, IR was used to characterize amino benzothiazole derivatives (**3a-e**). On the other hand, For the ease of NMR assignment of **4a-e**, all atoms of the scaffold are assigned by simple and prime numbers. It should be clarified that this numbering system is different from IUPAC numbering method. The numbered scaffold is provided in Scheme 1.

Benzo[d]thiazol-2-amine (3a)

White solid material, mp = 228-230 °C, IR (KBr) cm⁻¹: 3312, 3182 (N-H, str.), 3010 (C-H, aromatic, str.), 1624 (C=C, aromatic, str.), 1533

(C=N, str.), 1445 (C=C, aromatic, bend), 1195 (C-N, str.).

6-Fluorobenzo[d]thiazol-2-amine (3b)

Dark orange solid material, mp = 183-186 °C, IR (KBr) cm⁻¹: 3387, 3263 (N-H, str.), 3063 (C-H, aromatic, str.), 1634 (C=C, aromatic, str.), 1534 (C=N, str.), 1460 (C=C, aromatic, bend), 1251 (C-N, str.), 1185(C-F, str.).

6-Methoxybenzo[d]thiazol-2-amine (3c)

Orange solid material, mp = 166-170 °C, IR (KBr) cm⁻¹: 3406, 3360 (N-H, str.), 3103 (C-H, aromatic, str.), 2981 (C-H, aliphatic, str.), 1644 (C=C, aromatic, str.), 1548 (C=N, str.), 1460 (C=C, aromatic, bend), 1198 (C-O, str.), 1172 (C-N, str.).

6-Ethoxybenzo[d]thiazol-2-amine (3d)

Orange solid material, mp = 322-325 °C, IR (KBr) cm⁻¹: 3433, 3295 (N-H, str.), 3070 (C-H, aromatic, str.), 2725 (C-H, aliphatic, str.), 1638 (C=C, aromatic, str.), 1540 (C=N, str.), 1452 (C=C, aromatic, bend), 1262 (C-O, str.), 1201 (C-N, str.).

6-(Trifluoromethoxy)benzo[d]thiazol-2-amine (3e)

White solid material, mp = 119-120 °C, IR (KBr) cm⁻¹: 3564, 3381 (N-H, str.), 3096 (C-H, aromatic, str.), 1645 (C=C, aromatic, str.), 1538 (C=N, str.), 1464 (C=C, aromatic, bend), 1262 (C-O, str.), 1196 (C-N, str.), 1115 (C-F, str.).

4-[(Benzo[d]thiazol-2-ylimino) methyl]phenol (4a)

White crystalline solid, mp = 235-238 °C, IR (KBr) cm⁻¹: 2700-3350 (O-H, str.), 2946 (C-H, imine, str.), 1598 (C=C, aromatic, str.), 1581 (C=N, str.), 1485 (C=C, aromatic, bend), 1241 (C-O, str.), 1153 (C-N, str). ¹HNMR (DMSO-d_6): δ (ppm) 9.04 [s, 1H, OH], 8.03 [d, 1H, C7-H, J = 8 Hz], 7.96 [d, 2H, C2´-H, C6´-H, J = 8 Hz], 7.90 [d, 1H, C4-H, J = 4 Hz], 7.47-7.52 [m, 1H, C5-H], 7.37-7.41 [m, 1H, C6-H], 6.95 [d, 2H, C3´-H, C5´-H, J = 8 Hz]. ¹³CNMR (DMSO-d_6): δ 171.94(the carbon which is directly bonded to nitrogen and sulfur) (23), 166.45, 162.75, 151.38, 133.79, 132.72, 126.47, 125.80, 124.83, 122.21, 116.09. m/z: 254.05 (EI), yield 64%.

4-[((6-Fluorobenzo[d]thiazol-2-yl) imino) methyl]phenol (4b)

Dark orange crystalline solid, mp = 245-248 °C, IR (KBr) cm^{-1}: 2700-3300 (O-H, str.), 3066 (C-H, aromatic and imine, str.), 1601 (C=C, aromatic, str.), 1569 (C=N, str.), 1448 (C=C, aromatic, bend), 1231 (C-O, str.), 1195(C-N, str.), 1147 (C-F, str.); ^{1}HNMR (DMSO-d_6): δ 9.01 [s, 1H, OH], 7.89-7.99 [m, 5H, -CH=N, C7-H, C4-H, C2´-H, C6´-H], 7.34-7.39 [m, 1H, C6-H], 6.94-6.96 [d, 2H, C3´-H, C5´-H, J= 8 Hz]. ^{13}CNMR (DMSO-d_6): δ (ppm) 171.75, 166.56, 162.81, 160.52, 158.11, 148.13, 134.74, 132.75, 125.73, 123.47, 123.38, 116.10, 114.88, 114.64, 108.85, 108.58. m/z: 272.04, yield 70%.

4-[((6-Methoxybenzo[d]thiazol-2-yl) imino) methyl]phenol (4c)

Orange crystalline solid, mp = 243-245 °C, IR (KBr) cm^{-1}: 2500-3350 (O-H, str.), 3038 (C-H, aromatic and imine, str.), 2834 (C-H, aliphatic, str.), 1588 (C=C, aromatic, str.), 1520 (C=N, str.), 1465 (C=C, aromatic, bend), 1241 (C-O, str.), 1153 (C-N, str), ^{1}HNMR (DMSO-d_6): δ 8.97 [s, 1H, OH], 7.92-7.94 [d, 2H, C2´-H, C6´-H, J = 8 Hz], 7.79 [s, 1H, -CH=N], 7.77 [s, 1H, C7-H], 7.62 [s, 1H, C4-H], 7.07-7.10 [dd, 1H, C6-H, J =8 Hz, J´ = 4 Hz], 6.94 [d, 2H, C3´-H, C5´-H, J = 8 Hz]. ^{13}CNMR (DMSO-d_6): δ (ppm) 169.44, 165.38, 162.53, 157.02, 145.57, 135.06, 132.45, 125.88, 122.89, 116.05, 115.48, 105.04, 55.65. m/z: 284.06, yield 52%.

4-[((6-Ethoxybenzo[d]thiazol-2-yl) imino) methyl]phenol (4d)

Orange crystalline solid, mp = 250-253 °C,

IR (KBr) cm^{-1}: 2350-3400 (O-H, str.), 3029 (C-H, aromatic and imine, str.), 2857 (C-H, aliphatic, str.), 1601 (C=C, aromatic, str.), 1570 (C=N, str.), 1451 (C=C, aromatic, bend), 1208 (C-O, str.), 1155 (C-N, str), ^{1}HNMR (DMSO-d_6): δ 8.97 [s, 1H, OH], 7.93 [d, 2H, C2´-H, C6´-H, J = 8 Hz], 7.78 [s, 1H, -CH=N], 7.76 [s, 1H, C7-H], 7.60 [d, 1H, C4-H], 7.08-7.05 [dd, 1H, C6-H, J = 8 Hz, J´ = 4 Hz], 6.95 [d, 2H, C3´-H, C5´-H, J = 8 Hz], 4.12-4.07 [q, 2H, J = 8, -CH$_2$CH$_3$], 1.39-1.35 [t, 3H, J = 8 Hz, -CH$_2$CH$_3$]. ^{13}CNMR (DMSO-d_6): δ (ppm) 169.37, 165.33, 162.35, 156.27, 145.48, 135.08, 132.43, 125.99, 122.90, 116.00, 115.80, 105.61, 63.64, 14.62. m/z: 298.08, yield 65%.

4-[((6-(Trifluoromethoxy)benzo[d]thiazol-2-yl) imino)methyl]phenol (4e)

White crystalline solid, mp = 170-178 °C, IR (KBr) cm^{-1}: 2300-3400 (O-H, str.), 3038 (C-H, aromatic and imine, str.), 1603 (C=C, aromatic, str.), 1569 (C=N, str.), 1450 (C=C, aromatic, bend), 1242 (C-O, str.), 1193 (C-N, str.), 1149 (C-F, str), ^{1}HNMR (DMSO-d_6): δ 9.16 [s, 1H, OH], 8.32 [s, 1H, -C=N-], 8.10-8.07 [m, 4H, C2´-H, C6´-H, C4-H, C7-H], 7.62-7.59 [m, 1H, C6-H], 7.07 [d, 2H, C3´-H, C5´-H, J = 8 Hz]. ^{13}CNMR (DMSO-d_6): δ (ppm) 173.54, 167.12, 163.04, 150.30, 144.90, 134.90, 132.94, 125.64, 123.27, 120.24, 116.15, 115.41. m/z: 338.03, yield 45%.

DPPH radical scavenging activity assay

The percentage of DPPH scavenging activity for the studied compounds is shown in Fig. 1. IC$_{50}$ values calculated from the curves are mentioned in Table 1.
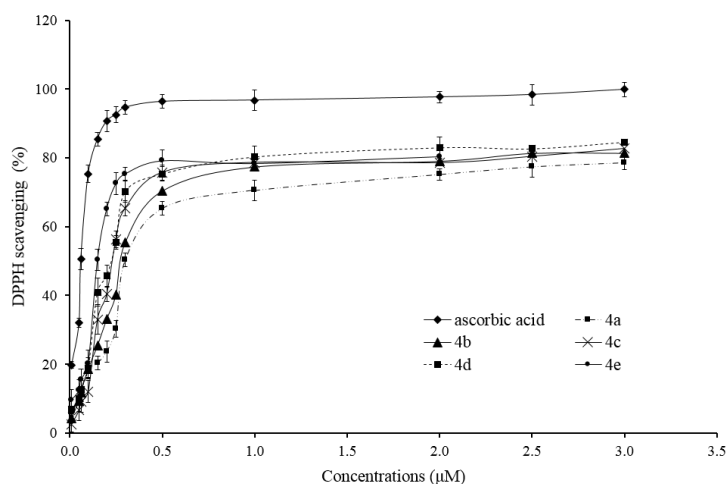

Fig. 1. The percentage of DPPH scavenging activity of the studied compounds at different concentrations. DPPH, 2,2-Diphenyl-1-picryl-hydrazyl-hydrate.

40

Table 1. Global parameters calculated at B3LYP/6-311++G** level of theory [eV] and IC_{50} values of the prepared compounds.

| Parameters	4a	4c	4d	4b	4e
Highest occupied molecular orbital energy	-6.32	-5.95	-5.95	-6.34	-6.50
Single occupied molecular orbital energy	-6.40	-6.08	-6.07	-6.31	-6.41
lowest unoccupied molecular orbital energy	-2.56	-2.22	-2.29	-2.24	-2.25
ΔE gap	3.76	3.73	3.66	3.75	4.25
Ionization potential	6.32	5.95	5.95	6.34	6.50
Electron affinity	2.56	2.22	2.29	2.24	2.25
Hardness	1.88	1.86	1.83	1.87	2.12
Softness	0.26	0.26	0.27	0.26	0.23
IC_{50}	0.3 ± 0.01	0.18 ± 0.01	0.14 ± 0.01	0.27 ± 0.01	0.24 ± 0.01

The order of DPPH scavenging activity (decreasing to the right) is as follows: ascorbic acid (0.074), **4d** (0.144 µM), **4c** (0.183 µM), **4e** (0.244 µM), **4b** (0.274 µM), and **4a** (0.3 µM). All of the studied compounds had lower antioxidant activity than ascorbic acid (< 0.05). Among them, compounds **4d** and **4c** possessed the best antioxidant potency in terms of DPPH scavenging effect.

Computational study results:
Frontier molecular orbitals of (benzo[*d*]thiazol-2-ylimino) methyl derivatives

To find the relationship between the electron delocalization and radical stability, SOMO shapes of electron distribution in radicals were provided in Fig. 2.

According to Fig. 2, the SOMO of electron distribution in radical species of **4a-e** is extended over the oxygenatom, benzene ring, and benzothiazole moiety. The electrons are slightly localized on the oxygen atom of the substituent, perhaps owing to the withdrawing effect of the oxygen atom on the substituent.
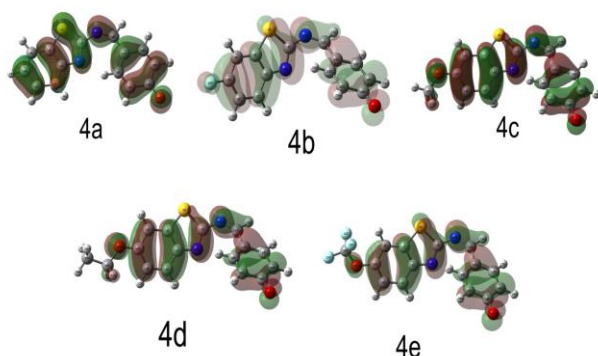
Fig. 2. The single occupied molecular orbital of electron distribution in rdical species of **4a-e**.

Global descriptive parameters for (benzo[d]thiazol-2-ylimino)methyl derivatives
HOMO and LUMO energies of the studied compounds at the level of B3LYP/6-311G** in the PCM phase are shown in Table 1. The values of E_{HOMO} for **4c** and **4d** among the studied compounds were closer to zero, thus, based on the *in silico* results; these compounds have the best scavenging activity.

The next electronic descriptor is the energy gap (E_{gap}) of E_{HOMO} and E_{LUMO}, which is also exploited to evaluate the affinity for losing an electron to form radical forms. Compound **4d** showed the lowest E_{gap} (Table 1) and it is shown that the lower E_{gap} leads to the easier electron leave from the molecule which produces radical forms in a less energetically manner (10). Thus, in theory, **4d** could be regarded to have the highest affinity for losing an electron to form radical forms. In contrast, **4e** (E_{gap} = 4.25) possessed the lowest affinity for losing electrons leading to the radical form.

The calculated SOMO energy of the produced radicals is reported in Table 1. The smallest amount of the SOMO energy belonged to **4c** and **4d** radicals. It means that they would be the most stable ones among the studied radicals.

The global η could be defined as the structure resistance to radical charge transfer while S indicates affinity to charge transfer. As shown in Table 1, **4e** had the highest η and lowest S.

To compare electron donation and electron abstraction, IP and EA were investigated and provided in Table 1. Higher IP could be concluded as the lower electron loss tendency. That is, an electron is removed from the HOMO of the neutral antioxidant molecule. this molecule changes to the radical c ation form. Lower IP leads to the stronger affinity to change to the radical cation form.

According to Tables 1, **4c** and **4d** showed the lowest amounts of IP values; i.e. the strongest donating capacity to form a radical cation, and **4e** had the lowest tendency to produce the radical cation form. EA can be expressed as the amount of energy released when an electron is abstracted. The greater EA of a molecule means accepts an electron from ROSs more easily than other molecules. Calculated EA for **4a-e** proved relatively higher values of EA for **4c-e** than **4a**.
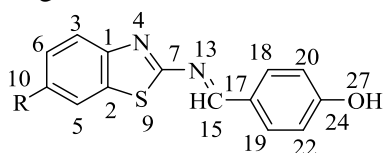
Fig. 3. Atom numbering scheme of the studied compounds used for perturbation theory analysis.

NBO analysis

The second-order perturbation theory analysis was performed. The atom numbering scheme of the studied compound is shown in Fig. 3 and the results of these calculations are provided in Table 2. In this scaffold, the π type electron system determines the stability of the , and the unpaired electrons of S and O-R substituents are mostly distributed to the -C7 and C5-C10 bonds, respectively. It seems that the oxygen lone pair electrons have resonance with the structure. Indeed, in **4c**, **4b,** and **4e**, the majority of π type electron system conjugations were shown but the smallest amount of conjugation was shown in **4d**.

Table 2. Perturbation theory analysis of the studied compounds.

Radicals	Type	Donor	Type	Acceptor	Energy [a] (Kcal/mol)
4a	ππ	C1-C2	π*	C5-C10	9.89
	π	C3-C6	π*	C1-C2	10.84
	π	C3-C6	π*	C5-C10	9.12
	π	N4-C7	π*	C1-C2	9.25
	π	C5-C10	π*	C3-C6	9.77
	π	N13-C15	π*	N4-C7	13.51
	π	C17-C19	π*	N13-C15	17.40
	π	C17-C 19	π*	C18-C20	12.94
	π	C18-C 20	π*	C22-C24	11.36
	LP (2)	C22-C 24	π*	C17-C19	24.21
		S	π*	N4-C7	13.90
4c	π	C1-C2	π*	C5-C10	10.02
	π	C3-C6	π*	C1-C2	9.53
	π	C3-C6	π*	C5-C10	10.05
	π	C5-C10	π*	C3-C6	10.23
	π	C5-C17	π*	C19-C24	16.24
	π	C5-C17	π*	C20-C26	14.37
	LP (2)	S	π*	N4-C7	13.20
	LP (2)	N13	π*	N4-C7	26.76
	LP (2)	N13	π*	C15-C17	49.56
	LP (2)	O-CH3	π*	C5-C10	13.12
4d	π	C3-C6	π*	C5-C10	11.41
	π	C5-C10	π*	C1-C2	12.58
	LP (2)	S	π*	N4-C7	11.34
	LP (2)	O-CH2-CH3	π*	C5-C10	16.21
4b	π	C1-C2	π*	C5-C10	10.27
	π	C3-C6	π*	C1-C2	10.02
	π	C3-C6	π*	C5-C10	10.38
	π	C5-C10	π*	C3-C6	9.16
	π	C17-C18	π*	N13-C14	17.16
	π	C17-C18	π*	C19-C22	12.75
	LP (2)	S	π*	C1-C2	9.46
	LP (2)	S	π*	N4-C7	13.45
4e	π	C1-C2	π*	C5-C10	10.29
	π	C3-C6	π*	C5-C10	10.11
	π	C17-C19	π*	N13-C14	17.07
	π	C17-C19	π*	C20-C26	12.67
	LP (2)	S	π*	N4-C7	13.50
	LP (2)	O-CF3	π*	C5-C10	10.23

[a] Energy of hyperconjugative interaction (stabilization energy).

In this scaffold, the π type electron system determines the stability of the radicals, and the unpaired electrons of S and O-R substituents are mostly distributed to the N4-C7 and C5-C10 bonds, respectively. It seems that the oxygen lone pair electrons have resonance with the structure. Indeed, in **4c**, **4b,** and **4e**, the majority of π type electron system conjugations were shown but the smallest amount of conjugation was shown in **4d**.

The radical electrons are distributed to the O-atom located in the para position, double bonds, imine bonds, and benzene ring. It is implied from Table 2 that there is a low extended conjugative interaction in **4d** and **4e** radicals. On the other hand, LP (2) of -OCH$_2$CH$_3$, -CH$_3$, -OCF$_3$ is delocalized with the C5-C10 bond of the structure. The highest stabilization energy was measured for **4d**. It should be noted that the electron-withdrawing properties of -OCF$_3$, -OCH$_3$, and -OCH$_2$-CH$_3$ is promoted through the resonance.

Antioxidant capacity

The preferred antioxidant mechanism can be characterized utilizing BDE, IP, and PDE values of the studied compounds (Table 3). The possible HAT mechanism can be investigated in accordance with the enthalpies of the homolytic O-H bond cleavage; it points to the BDE values obtained for the (benzo[*d*]thiazol-2-ylimino)methyl derivatives. In the HAT mechanism (I), the lower BDE values are associated with higher antioxidant activity. Table 3 implies that the homolytic cleavage of the phenol hydroxyl moiety bond in **4d** is slightly favored.

To explain the observed experimental data, SET-PT mechanism was also investigated. In the first step of SET-PT reactions, the neutral compound (ArOH) is converted to a radical cation. For better comparison, the values of an AIP of the O-H bond cleavage in PCM phase were calculated. It implies that heterolytic

cleavage of the phenol hydroxyl bond in the neutral form of **4d** is favored. According to this parameter, the probability of radical cation formation from the corresponding neutral phenol hydroxyl bond in **4d** is high, while the radical cation formation in **4a** is very improbable. The AIP parameter values are not in agreement with the experimental results. In the second step of the SET-PT mechanism, the radical cation form converts to the neutral radical. Here, the enthalpies of the heterolytic O-H bond cleavage were used to calculate the PDE. The PDE values for heterolytic O-H bond cleavage in the phenol hydroxyl group of the radical cation species in the PCM phase were calculated. The results imply that the heterolytic cleavage of the 3-OH bond in the radical cation form of **4a** is strongly favored. The probability of the neutral radical formation from the corresponding radical cation (II) is very low for the studied compounds and the lowest for **4c**. This step of the SET-PT mechanism is almost improbable for **4a**. Furthermore, the PDE parameter results are not in agreement with the experimental data.

SPLET mechanism has also been examined to find out the possible mechanism of the antioxidant activity of the studied compounds. In the first step of this mechanism (III), ionization of the phenol hydroxyl group in the PCM phase occurs. PA enthalpy is a value which is used for describing the SPLET mechanism. The calculated PA values imply that the heterolytic cleavage of the 3-OH bond and proton release in **4d** is strongly preferred. It is evident that the probability of the anion formation (III) on the phenolic hydroxyl is the most for **4d**, and the least for **4c**, a computational finding which is in agreement with the experimental data provided in Table 1.

The second step of the SPLET antioxidant mechanism is the formation of a neutral radical from the anion. To explain this step, ETE values are usually exploited. Radical formation on the phenol hydroxyl is preferred for **4c** and **4d** (20).

Table 3. Calculated energies for the steps of different mechanisms of scavenging activity. (kJ/mol, at 298.15 K, PCM, B3LYP/6-311++G** level of theory).

Molecules	Bond dissociation enthalpy	Adiabatic ionization potential	Proton dissociation enthalpy	Proton affinity	Electron transfer enthalpy
4a	1662	581	1080	163	477
4c	1660	534	1125	175	463
4d	1654	530	1124	159	473
4b	1665	565	1100	161	482
4e	1672	573	1098	166	483
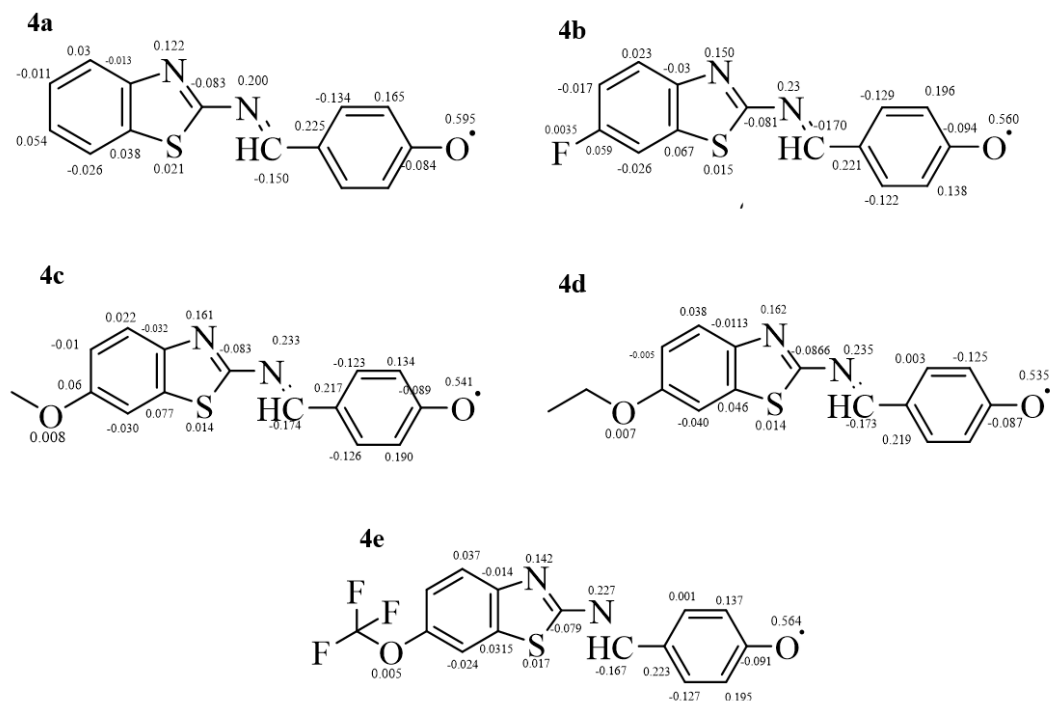
Fig. 4. Distribution of the spin densities and the amounts of spin densities in the radical species formed by H-removal from the neutral forms of **4a-e**.

Spin density analysis

In radical species of **4a-e** arising H- removal from the OH group (I), the spin density distribution is delocalized to some extent on the O atom, benzene ring, and benzothiazole moiety (Fig. 4). In order to rationalize the differences in the reactivity of the OH groups, the amounts of the spin density distribution on the radical species of **4a-e** were determined. For **4a**, the spin density appears to be less delocalized for the radical originating from the phenolic OH than other structures. The spin population on the O-atom in the **4a** radical species is 0.595 and 0.560, 0.541, 0.535, and 0.564 for the same position in **4b**, **4c**, **4d,** and **4e**, respectively (Fig. 4). The spin density distribution is the lowest on the benzene ring atom to which the hydroxyl group is attached. Besides, the spin density distribution on S-atom in the **4a** radical is 0.021 and 0.015, 0.014, 0.014, and 0.017 in the radical forms of **4b**, **4c**, **4d,** and **4e**, respectively. Based on the spin density distribution results **4d** possess high antioxidant activity.

DISCUSSION

In 2003, DFT calculation was applied to study structure-activity of resveratrol (24). The resveratrol molecular geometry was optimized using B3LYP/6-31G** then its HOMO, LUMO, and its radical spin density distribution were investigated. It was found that the resonance effect plays an important role in the stability of the formed radicals. Indeed, it seems that the antioxidant activity of resveratrol is related to the spin density and the unpaired electron distribution of the O-atom (24). According to the study published in 2013;the theoretical antioxidant pharmacophores for resveratrol is the 4-hydroxystilbene (10).

Considering the concept of bioisosterism; **4a-e** were designed equivalent to the 4-hydroxystilbene moiety. The benzothiazole part was conjugated to another part to recognize Aβ. The study published in 2017 confirmed that elongation of the conjugated bridges in resveratrol similar scaffolds leads to further improvement in its antioxidant activity (25).

According to the second-order perturbation theory analysis, more conjugation causes more delocalization and more stability of the radical electron in the radical species. The antioxidant activity of this scaffold is related to the stabilization energy released through the conjugation. Thus, the stabilization energy in these scaffolds especially **4c** is the most,

although **4b**, **4e** showed high stabilization energy and extended delocalization (25). According to the DPPH scavenging activity for the studied compounds, it is obvious that the introduction of a substituent on the **4a** structure changed the antioxidant activity of the parent compound. It seems that the insertion of electron-withdrawing substituents in compounds **4b** and **4e** has reduced the activity. Substituents with less electron-withdrawing character in **4d** and **4c** had increased radical scavenging activity among the studied compounds. In this structure, similar to resveratrol scaffolds, the π-type electron delocalization determines the radical stability which is mostly distributed to the O-atom, double bond, and B-benzene ring. According to the SOMO of radical species, it appears that the designed compounds would have a good radical scavenging activity. Furthermore, SOMO of -OCH$_3$, -OCH$_2$CH$_3$, and -OCF$_3$ refers to the more delocalization of electrons in all the studied compounds. In fact, *para* substitution on the benzothiazole ring with these groups increases the SOMO shapes of electron delocalization (24).

In theoretical studies, it is demonstrated that E$_{HOMO}$ is a valid descriptor of the scavenging activity. If the E$_{HOMO}$ is less negative (closer to zero) it actually indicates that the structure is more unstable and an electron has more affinity to leave the molecule. E$_{HOMO}$ values were compared with resveratrol and some well-known natural antioxidants, *e.g.* 3-methoxy-4-hydroxycumarin, apigenin, scutellarein, and aleo-emodin (26). The E$_{HOMO}$ for resveratrol and **4d** were calculated to be 5.48 and -5.98 ev, respectively. Indeed, **4d** showed E$_{HOMO}$ value near to other antioxidants. E$_{HOMO}$ for 3-methoxy-4-hydroxy curcumin, apigenin, scutellarein were obtained -0.25, -6.15, -5.93 eV, respectively. It seems that **4d** can be considered as a promised antioxidant. Indeed, it was revealed that **4d** showed the lowest E$_{gap}$. **4e** possessed the lowest affinity for charge transfer. Other studied structures showed similar affinities to charge transfer. It may be because of the powerful electron-withdrawing effect of -OCF$_3$ moiety in the structure of **4e**. The electrons are slightly localized on the oxygen atom of the -OCF$_3$ substituent. This

electron localization increased global η. These data are in accordance with E$_{gap}$ values. It implies that **4e** showed the lowest affinity for electron loss, explained by the localization of the electrons on the oxygen atom of the -OCF$_3$ (19).

Furthermore, theoretical predictions for the HAT and SPLET mechanisms are more consistent with the experimental data. The data shown in Table 3 indicate that the lowest energy barriers belong to the SPLET mechanism. The first step of this mechanism (PA) has relatively low barriers, about 160-170 kJ/mol for compounds **4a** to **4e**. Indeed, the probability for the second step of this mechanism is quite low, again a high barrier is observed for the **4b** and **4e**. Other mechanisms, *i.e.* HAT (BDE parameter) and SET-PT (AIP) have barriers for the first step, always higher than 500 kJ/mol. It can be noticed that the second step of the SET-PT has very high energy barriers (PDE). The high AIP values point out that this mechanism cannot effectively explain the antioxidant activity. Therefore, SPLET is the most possible mechanism for the radical scavenging activity of the studied compounds.

This method is solvent-dependent due to the formation of charged species. Solvation, pKa, and the possibility of charged species formation have major effects on this mechanism. The Mulliken spin density distribution is the most reliable parameter which provides a better description of the stability and reactivity of the **4d** and **4c** (27). The higher stability of **4c** and **4d** corresponds to better efficiency of the antioxidant because it is improbable to react with other ROS (28,29).

CONCLUSION

Experimental and theoretical methodologies were adopted to study geometry and antioxidant properties of (benzo[*d*]thiazol-2-ylimino) methyl derivatives against ROSs in Alzheimer's disease. E$_{HOMO}$ and E$_{gap}$ were calculated and compared with resveratrol parameters. **4d** was recognized as the softest molecule. In contrast, **4e** showed resistance against the electron transfer and electron delocalization. DPPH scavenging activity was in agreement with the theoretical results.

The second-order perturbation theory showed that **4c-e** radicals are strongly stabilized *via* hyperconjugation. The SPLET mechanism is recognized as the preferred antioxidant mechanism. This mechanism seriously depends on the experimental medium. PCM stabilized ionization of the 3-OH. This method is solvent dependent due to the formation of charged species. The spin density distribution of the unpaired electron on ArO was analyzed and **4c-d** had the highest distribution. In sum, insertion of -OCH$_3$, -OCH$_2$CH$_3$, and -OCF$_3$ to the benzo[*d*]thiazol-2-ylimino) methyl scaffold promotes its anti-oxidant activity.

Acknowledgments

Conflict of interest statement

The authors declared no conflicts of interest in this study.

Authors' contribution

The idea was developed by A. Fassihi. M.H. Asgarshamsi designed the DFT study. A. Movahedian supervised the DPPH study. Data collection and analysis was performed by A. Fassihi and H. Mohammad beigi. F. Hasanzadeh and L. Saghaei contributed to manuscript preparation and revision.

REFRENCES

1. Das TK, Wati MR, Fatima-Shad K. Oxidative stress gated by Fenton and Haber Weiss reactions and its association with Alzheimer's disease. Arch Neurosci. 2015;2(2):e20078.
   DOI: 10.5812/archneurosci.20078.
2. Luan S, Yun X, Rao W, Xiao C, Xu Z, Lang J, *et al*. Emamectin benzoate induces ROS-mediated DNA damage and apoptosis in Trichoplusia Tn5B1-4 cells. Chem Biol Interact. 2017;273:90-98.
   DOI: 10.1016/j.cbi.2017.06.004.
3. Sinha MS, Ansell-Schultz A, Civitelli L, Hildesjö C, Larsson M, Lannfelt L, *et al*. Alzheimer's disease pathology propagation by exosomes containing toxic amyloid-beta oligomers. Acta Neuropathol. 2018;136(1):41-56.
   DOI: 10.1007/s00401-018-1868-1.
4. Luo J, Wärmländer SK, Gräslund A, Abrahams JP. Cross-interactions between the Alzheimer disease amyloid-β peptide and other amyloid proteins: a further aspect of the amyloid cascade hypothesis. J Biol Chem. 2016;291(32):16485-16493.
   DOI: 10.1074/jbc.R116.714576.
5. Bredesen DE. Metabolic profiling distinguishes three subtypes of Alzheimer's disease. Aging (Albany NY). 2015;7(8):595-600.
   DOI: 10.18632/aging.100801.
6. Strodel B, Coskuner-Weber O. Transition metal ion interactions with disordered amyloid-β peptides in the pathogenesis of alzheimer's disease: insights from computational chemistry studies. J Chem Inf Model. 2019;59(5):1782-1805.
   DOI: 10.1021/acs.jcim.8b00983.
7. Lu C, Guo Y, Li J, Yao M, Liao Q, Xie Z, *et al*. Design, synthesis, and evaluation of resveratrol derivatives as Aß1-42 aggregation inhibitors, antioxidants, and neuroprotective agents. Bioorg Med Chem Lett. 2012;22(24):7683-7687.
   DOI: 10.1016/j.bmcl.2012.09.105.
8. Mishra CB, Manral A, Kumari S, Saini V, Tiwari M. Design, synthesis and evaluation of novel indandione derivatives as multifunctional agents with cholinesterase inhibition, anti-β-amyloid aggregation, antioxidant and neuroprotection properties against Alzheimer's disease. Bioorg Med Chem. 2016;24(16):3829-3841.
   DOI: 10.1016/j.bmc.2016.06.027.
9. Xue C, Lin TY, Chang D, Guo Z. Thioflavin T as an amyloid dye: fibril quantification, optimal concentration and effect on aggregation. R Soc Open Sci. 2017;4(1):160696,1-12.
   DOI: 10.1098/rsos.160696.
10. Benayahoum A, Amira-Guebailia H, Houache O. A DFT method for the study of the antioxidant action mechanism of resveratrol derivatives. J Mol Model. 2013;19(6):2285-2298.
    DOI: 10.1007/s00894-013-1770-7.
11. Peerannawar S, Horton W, Kokel A, Török F, Török M, Török B.. Theoretical and experimental analysis of the antioxidant features of diarylhydrazonees. Struct Chem. 2017;28(2):391-402.DOI: org/10.1007/s11224-016-0867-x.
12. Jimonet P, Audiau F, Barreau M, Blanchard JC, Boireau A, Bour Y, *et al*. Riluzole series. Synthesis and *in vivo* "antiglutamate" activity of 6-substituted-2-benzothiazolamines and 3-substituted-2-imino-benzothiazolines. J Med Chem. 1999;42(15):2828-2843.
    DOI: 10.1021/jm980202u.
13. Tonelli A, Candiani A, Sozzi M, Zucchelli A, Foresti R, Dall'Asta C, *et al*. The geek and the chemist: antioxidant capacity measurements by DPPH assay in beverages using open source tools, consumer electronics and 3D printing. Sens Actuators B Chem. 2019;282:559-566.
    DOI: 10.1016/j.snb.2018.11.019.
14. Chong DP. MP2 or B3LYP: computed bond distances compared with CCSD (T)/cc-pVQZ. Can J Chem. 2018;96(3):336-339.
    DOI: 10.1139/cjc-2017-0651.

15. Gaussian 03, Revision C.02, Frisch M, Truck G,Schlegel H, Scuseria G, Robb M, Cheeseman J, *et al*. Gaussian Inc.,Wallingford CT,2004.

16. Galano A, Mazzone G, Alvarez-Diduk R, Marino T, Alvarez-Idaboy JR, Russo N. Food antioxidants: chemical insights at the molecular level. Annu Rev Food Sci Technol. 2016;7:335-352.
DOI: 10.1146/annurev-food-041715-033206.

17. Temel E, Alaşalvar C, Gökçe H, Güder A, Albayrak Ç, Alpaslan YB, *et al*. DFT calculations, spectroscopy and antioxidant activity studies on (E)-2-nitro-4-[(phenylimino) methyl] phenol. Spectrochim Acta A Mol Biomol Spectrosc. 2015;136(Part B):534-546.
DOI: 10.1016/j.saa.2014.09.067.

18. Choudhary V, Bhatt A, Dash D, Sharma N. DFT calculations on molecular structures, HOMO-LUMO study, reactivity descriptors and spectral analyses of newly synthesized diorganotin (IV) 2-chloridophenylacetohydroxamate complexes. J Comput Chem. 2019;40(27):2354-2363.
DOI: 10.1002/jcc.26012.

19. Nazifi SMR, Asgharshamsi MH, Dehkordi MM, Zborowski KK. Antioxidant properties of *Aloe vera* components: a DFT theoretical evaluation. Free Radic Res. 2019;53(8):922-931.
DOI: 10.1080/10715762.2019.1648798.

20. Marković Z, Milenković D, Đorović J, Marković JMD, Stepanić V, Lučić B, *et al*. PM6 and DFT study of free radical scavenging activity of morin. Food Chem. 2012;134(4):1754-1760.
DOI: 10.1016/j.foodchem.2012.03.124.

21. Boulebd H. DFT study of the antiradical properties of some aromatic compounds derived from antioxidant essential oils: C-H bond *vs.* O-H bond. Free Radic Res. 2019;53(11-12):1125-1134.
DOI: 10.1080/10715762.2019.1690652.

22. Ali HM, Ali IH. A DFT and QSAR study of the role of hydroxyl group, charge and unpaired-electron distribution in anthocyanidin radical stabilization and antioxidant activity. Med Chem Res. 2017;26:2666-2674.
DOI: 10.1007/s00044-017-1964-0.

23. Alishahi N, Nasr-Esfahani M, Mohammadpoor-Baltork I, Tangestaninejad S, Mirkhani V, Moghadam M. Nicotine-based ionic liquid supported on magnetic nanoparticles: an efficient and recyclable catalyst for selective one-pot synthesis of *mono*-and *bis*-4*H*-pyrimido [2,1-*b*] benzothiazoles. Appl Organometal Chem. 2020;34(8):e5681,1-14.
DOI: 10.1002/aoc.5681.

24. Cao H, Pan X, Li C, Zhou C, Deng F, Li T. Density functional theory calculations for resveratrol. Bioorg Med Chem Lett. 2003;13(11):1869-1871.
DOI: 10.1016/s0960-894x(03)00283-x.

25. Lu L, Zhu S, Zhang H, Zhang S. Improvement of antioxidative activity of resveratrol by elongating conjugated chain: a DFT theoretical study. Comput Theor Chem. 2013;1019:39-47.
DOI: 10.1016/j.comptc.2013.06.019.

26. Sadasivam K, Kumaresan R. A comparative DFT study on the antioxidant activity of apigenin and scutellarein flavonoid compounds. Mol Phys. 2011;109(6):839-852.
DOI: 10.1080/00268976.2011.556576.

27. Anouar EH, Shah SAA, Hassan NB, Moussaoui NE, Ahmad R, Zulkefeli M, *et al*. Antioxidant activity of hispidin oligomers from medicinal fungi: a DFT study. Molecules. 2014;19(3):3489-3507.
DOI: 10.3390/molecules19033489.

28. Samimi F, Baazm M, Eftekhari E, Rajabi S, Goodarzi MT, Jalali Mashayekhi F. Possible antioxidant mechanism of coenzyme Q10 in diabetes: impact on Sirt1/Nrf2 signaling pathways. Res Pharm Sci. 2019;14(6):524-533.
DOI: 10.4103/1735-5362.272561

29. Sadeghi M, Safaiean L, Aghaye Ghazvini M, Ramezani M. Evaluation and fibrinolytic and antioxidant effect of *Allium affine* hydrochloric extract. Res Pharm Sci.2017;12(4):299-306.
DOI: 10.4103/1735-5362.212047.